

# Modeling the Dynamics of Bivalent Histone Modifications

Wai Lim Ku<sup>1,2\*</sup>, Michelle Girvan<sup>1,2,3</sup>, Guo-Cheng Yuan<sup>4,5</sup>, Francesco Sorrentino<sup>6</sup>, Edward Ott<sup>1,2,7</sup>

**1** Department of Physics, University of Maryland, College Park, Maryland, United States of America, **2** Institute for Research in Electronics and Applied Physics, University of Maryland, College Park, Maryland, United States of America, **3** Institute for Physical Science and Technology, University of Maryland, College Park, Maryland, United States of America, **4** Department of Biostatistics, Harvard School of Public Health, Boston, Massachusetts, United States of America, **5** Department of Biostatistics and Computational Biology, Dana-Farber Cancer Institute, Boston, Massachusetts, United States of America, **6** Department of Mechanical Engineering, University of New Mexico, Albuquerque, New Mexico, United States of America, **7** Department of Electrical and Computer Engineering, University of Maryland, College Park, Maryland, United States of America

## Abstract

Epigenetic modifications to histones may promote either activation or repression of the transcription of nearby genes. Recent experimental studies show that the promoters of many lineage-control genes in stem cells have “bivalent domains” in which the nucleosomes contain both active (H3K4me3) and repressive (H3K27me3) marks. It is generally agreed that bivalent domains play an important role in stem cell differentiation, but the underlying mechanisms remain unclear. Here we formulate a mathematical model to investigate the dynamic properties of histone modification patterns. We then illustrate that our modeling framework can be used to capture key features of experimentally observed combinatorial chromatin states.

**Citation:** Ku WL, Girvan M, Yuan G-C, Sorrentino F, Ott E (2013) Modeling the Dynamics of Bivalent Histone Modifications. PLoS ONE 8(11): e77944. doi:10.1371/journal.pone.0077944

**Editor:** Jordi Garcia-Ojalvo, Universitat Politecnica de Catalunya, Spain

**Received:** June 13, 2013; **Accepted:** September 5, 2013; **Published:** November 1, 2013

**Copyright:** © 2013 Ku et al. This is an open-access article distributed under the terms of the Creative Commons Attribution License, which permits unrestricted use, distribution, and reproduction in any medium, provided the original author and source are credited.

**Funding:** This work was supported by Office of Naval Research grant N000140710734 and United States National Institutes of Health grant HG005085. The funders had no role in study design, data collection and analysis, decision to publish, or preparation of the manuscript.

**Competing Interests:** The authors have declared that no competing interests exist.

\* E-mail: wlku@umd.edu

## Introduction

Histones can undergo various types of covalent modifications, such as methylation and acetylation, which serve as an additional layer of transcriptional control by mediating the chromatin accessibility and by recruiting regulatory proteins [1,2]. Experimental studies using chromatin immunoprecipitation followed by massively parallel sequencing (ChIP-seq) have suggested that different cell types can be characterized by different histone modification patterns [3].

The molecular mechanisms underlying chromatin state establishment, maintenance, and heritability remain incompletely understood. A number of mechanisms are implicated [4], including (1) sequence-specific recruitment through interactions between chromatin regulators and DNA binding factors; (2) recruitment of chromatin regulators to existing histone marks; (3) histone marks deposited by transcriptional machineries; (4) RNA mediated recruitment; and (5) stochasticity associated with DNA replication. However, any single mechanism alone is insufficient for chromatin state establishment [4,5].

One of the best characterized chromatin states is a bivalent domain, a segment of the nucleosome array, in which H3K4me3 (an active mark) and H3K27me3 (a repressive mark) coexist on most individual nucleosomes within the domain [6]. Bivalent domains are thought to be an important feature of stem cells. For example, bivalent domains have been discovered in the promoters of most lineage-control genes in embryonic stem cells, and most of these domains become monovalent upon cell differentiation [3,6–9]. Also, a recent study observed that gene activation in the

differentiation process occurs in conjunction with the decay of repressive marks in bivalent domains [10]. In particular, one prominent proposal [6] for the function of bivalent domains is that the H3K27me3 marks act to repress the lineage-control gene in stem cells, while the H3K4me3 marks poise these genes for activation upon cell differentiation. Thus this proposal suggests that activation of these genes in differentiated cells is determined by the existence of bivalent domains in stem cells. These findings indicate the importance of bivalent domains and motivate further study in order to illuminate the underlying principles and mechanisms involved in their formation and evolution.

It has been proposed that the formation of chromatin domains is consistent with a model that includes not only the chemical interactions between histone marks, but also nucleation sites where domains are more likely to form [11]. The dynamics of histone modifications have been studied both theoretically and experimentally for some time [11–15]. In general, histone methylation marks are catalyzed by a variety of methyltransferase enzymes which may act singly or cooperatively. For example, H3K27me3 marks are catalyzed by Ezh2, a core member of the Polycomb group proteins. In addition to the normal stochastic conversion which would be expected from each of these individual enzymes, there is also a feedback process between the histone marks and the enzymes [16]. Existing H3K27me3 marks may attract Polycomb group complexes, which enhance nearby methylation [17,18]. A similar recruitment mechanism has also been suggested for H3K4me3 via Trithorax protein complexes (TrxG) [19]. In addition, there exists experimental evidence supporting a negative

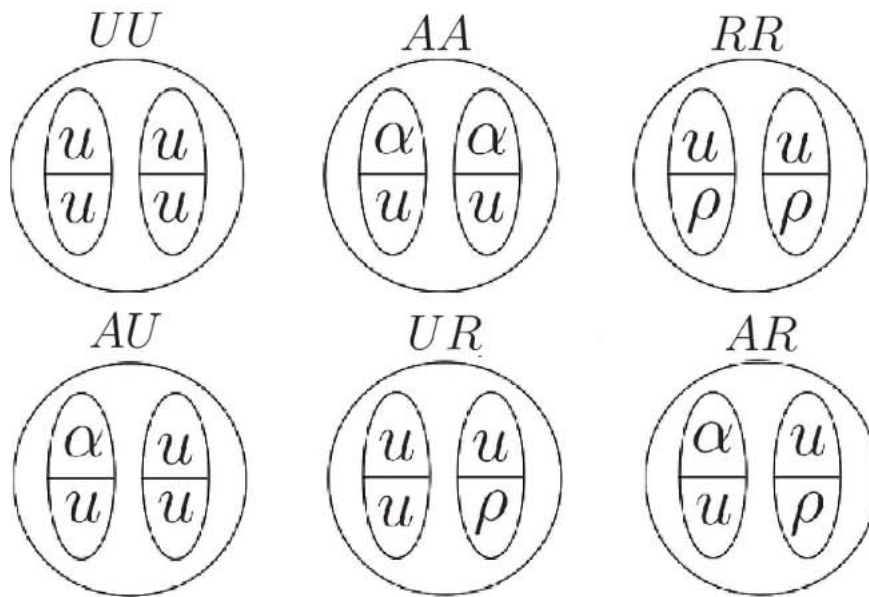


**Figure 1. 6-state model.** Illustration of the states in the 6-state model. Circles represent nucleosomes. A nucleosome contains two histones copies represented by the vertically oriented ellipses. Each histone has two sites, one site (represented by the upper half of the ellipse) that can be either unmodified (symbolized by  $u$ ) or have an active mark (symbolized by  $\alpha$ ), and another site (represented by the lower half of the ellipse) that can be either unmodified (symbolized by  $u$ ) or have a repressive mark (symbolized by  $\rho$ ). (Note that the physical nucleosome states labeled  $AU$ ,  $UR$  and  $AR$  could be just as well depicted by interchanging the left and right ellipses within the respective circles.)  
doi:10.1371/journal.pone.0077944.g001

feedback mechanism between H3K4me3 and H3K27me3 marks via the action of histone demethylases[20–24].

Certain specific DNA sequences may serve as the docking sites of modification enzymes and may therefore be associated with enhanced local attraction of histone marks [4,25]. We refer to these as nucleation sites. For example, CpG islands are strongly enriched in bivalent domains in human and mouse embryonic stem cells [19], and appear to be required for Polycomb binding in certain cases [26].

Recently, *in silico* methods have provided important additional insights for chromatin state inheritance. Major contributions have been made by Dodd et al. [12] and Sedighi and Sengupta [27]. These paper considered 1-dimensional lattice models in which nucleosomes are allowed to have active or repressive modifications that evolve stochastically and by recruitment. They found that a bistable state with either mostly active nucleosomes or mostly repressive nucleosomes can appear and be heritable, consistent with experimental observations. Subsequently, Hodges and Crabtree [11] found that adding a nucleation site into a model of the above type produces a bounded chromatin domain. Also, in a more recent paper, Binder et al. [28] proposed a model describing binding of catalytic enzymes to DNA and their interaction with histone marks with one aim being explaining length distributions of modified chromatin regions. These past studies are limited to a single type of histone mark on a nucleosome, whereas it is well-known that gene regulation is governed by combinatorial patterns of multiple histone marks [2,29]. In this paper, we extend previous studies by presenting an approach to model the dynamics of combinatorial chromatin states. This is achieved by allowing each individual nucleosome to carry both active and repressive marks simultaneously.

In the next section we describe our model. Then, in the Results section, we apply this model to investigate the dynamics of histone modification patterns with the focus on bivalent domains. Discussion and Conclusions are given at the end of the paper.

## Methods

### General Framework of our Model

We consider a 1D lattice of  $N$  nucleosomes, where there is a nucleosome at each lattice site  $i = 1, 2, \dots, N$ . An actual nucleosome consists of 8 histone protein molecules, that can be regarded as two identical groups of four each. In what follows we only consider the state of one of these four histone group members, namely the H3 histone, which is specifically related to bivalency. Thus, in our model, we represent the state of a nucleosome as being determined by the states of its two H3 histone copies. There are two modification sites in each H3 histone, one which may have an active mark (such as H3K4me3) and the other which may have a repressive mark (such as H3K27me3). Thus, there are 16 possible states of a nucleosome, and each of which is determined by 4 histone modification sites (see Figure S1). As shown in Text S1, this, together with the restriction obtained from experiment [30] that active and repressive marks do not occur simultaneously on the same H3 histone, leads to the six physically distinct nucleosome states depicted in Fig. 1. In Fig. 1 the circle represents a nucleosome and the vertical ellipses represent H3 histones. The lower case letters within each ellipse represent the states of the two modification sites of the H3 histone ( $u$  = unmodified,  $\alpha$  = modified by an active mark,  $\rho$  = modified by a repressive mark). For convenience, we assign the symbols  $UU$ ,  $AA$ ,  $RR$ ,  $AU$ ,  $UR$ , and  $AR$  to the six possible states. From now on, when we say ‘histone’ it is to be understood that we mean an H3 histone. We note that the state  $AR$  will play a prominent role in subsequent considerations in the Results section, and we will call a nucleosome in this state a ‘bivalent nucleosome’.

We then allow each nucleosome state to evolve according to a discrete time ( $t$ ) model, in which from time  $t$  to time  $t+1$ , a nucleosome state changes from state  $\sigma$  to state  $\sigma'$  with probability  $\pi_{\sigma\sigma'}$ . Since the time step  $t \rightarrow t+1$  is regarded as small, we assume that, at most, only one modification site may change on each time

step. Thus, there are 12 possible transitions among the 6 distinct states (see Fig. 2 which shows the possible transitions).

**Reduced Model**

The general framework above can lead to a relatively complex class of models and has many parameters. Thus, for the simulations that we report in this paper, we have adopted the somewhat modest goal of illustrating different types of dynamics that can arise when different nucleosome states interact and compete. With this goal in mind, we now seek an illustrative, but still somewhat plausible, reduction of our general 6-state model. Our reduction is based on the assumption, motivated in Text S1, that the occurrence of nucleosome states having either active marks on both histones (*AA* in Fig. 1) or repressive marks on both histones (*RR* in Fig. 1) are unlikely. Thus we consider the idealized case where *AA* and *RR* states do not occur. Hence each nucleosome of the reduced model is in only one of 4 nucleosome states, namely *AU*, *UR*, *AR* and *UU* (see Fig. 3A). Referring to Fig. 1, we see that the four states have the following meanings.

*AU*: One histone has an active mark and the nucleosome's other three sites are unmodified.

*UR*: One histone has a repressive mark and the nucleosome's other three sites are unmodified.

*AR*: One histone has an active modification, while its other site is unmodified. The other histone has a repressive modification, while its other site is unmodified.

*UU*: All four sites of the nucleosome are unmodified.

**Model Dynamics**

During a cell cycle, we consider the time *t* states of modeled nucleosomes on our one dimensional lattice and update these states to new states at time *t*+1 through two probabilistic processes that we call "recruitment conversion" and "exchange conversion". At the conclusion of a cell cycle, "replication" occurs, following which a new cycle begins.

**N Recruitment.** This refers to the recruitment of histone marks to a nucleosome through interaction with neighboring nucleosomes. Recruitment at a site *i* depends on the states of the nucleosomes in an interval of length *2l* centered at *i*, and we refer to *l* as the range of recruitment. We define  $f_X^i$  as the fraction of nucleosomes in this interval which carry a type-*X* histone mark, where the subscript  $f_X^i$  is *X* = *A*, *R*. If  $l \ll N-l$ , then the recruitment range will span *2l*+1 nucleosomes on our lattice. However, if *i* is too close to the

beginning or the end of the lattice (i.e.,  $1 \ll i \ll l$  or  $N-l \ll i \ll N$ , respectively), then the recruitment range will include 'phantom' sites *j* not on the lattice ( $j \ll 1$  and  $j \gg N$ , respectively), and for the purpose of determining  $f_X^i$ , we consider such phantom sites *j* to be in the *UU* state. The probability of recruitment conversion from *U* to *X* at site *i* is taken to be given by  $f_X^i r_{UX}$ , where  $r_{UX}$  is a constant describing the strength of the recruitment interaction. On the other hand, the probability of recruitment conversion from *X* to *U* (i.e., mark removal) depends on the concentration of histone marks which are opposite (rather than similar) to *X* (where we regard *A* and *R* as opposites). In this case, the conversion probability is taken to be given by  $f_Y^i r_{XU}$ , where *Y* is *R* if *X* is *A* and vice versa (see Fig. 3B). Note that in our model we allow  $r_{XU}$  to differ from  $r_{UX}$  because different enzymes are recruited for the addition and removal of histone marks.

**N Exchange.** Unlike the recruitment process, the exchange process refers to histone modifications which occur spontaneously, independent of the states of nearby nucleosomes. The probabilities for exchange conversion are denoted by  $p_{UA}$ ,  $p_{UR}$ ,  $p_{AU}$ , and  $p_{RU}$  (see Fig. 3C). In particular, we think of  $p_{AU}$  and  $p_{RU}$  as corresponding to the histone turnover process, and  $p_{UA}$  and  $p_{UR}$  as corresponding to processes involving nucleation sites (See Table 1).

**N DNA replication.** When DNA replication occurs, we imagine that in the real situation the parental nucleosomes are randomly assigned to one of the two daughter strands at the same site as that which they occupied on the parental strand, while the corresponding site on the other strand is assigned an unmodified nucleosome (i.e., a nucleosome in the *UU* state). This scenario is supported by an experimental observation [31]. In our model, we do not follow both daughter strands. Rather we follow just one. Thus, with probability 1/2, our model replication process randomly replaces each nucleosome with an unmodified (*UU*) nucleosome. This model DNA replication occurs periodically with a period equal to the 'cell cycle time'  $\tau$ . This is similar to how replication is modeled in [12].

In accord with the above recruitment and exchange processes, during a cell cycle, our model gives appropriate equations for the probabilities  $P_{XY}^i(t+1)$  that nucleosome *i* is in state *XY* = *UU*, *AU*, *UR*, *AR* at time *t*+1, given the state of the lattice at time *t*. After the probabilities  $P_{XY}^i(t+1)$  are determined the state (*UU*, *AU*, *UR* or *AR*) of each nucleosome *i* is randomly chosen according to the probabilities  $P_{XY}^i(t+1)$ , thus determining the state at time *t*+1. Letting  $\delta_{XY}^i(t) = 1$  if nucleosome *i* is in state *XY*, and  $\delta_{XY}^i(t) = 0$  if nucleosome *i* is not in state *XY*, our model equations for the probabilities are

$$P_{AU}^i(t+1) = 2[f_A^i(t)r_{UA} + p_{UA}^i]\delta_{UU}^i(t) + [f_A^i(t)r_{RU} + p_{RU}] \delta_{AR}^i(t) + \{1 - [f_R^i(t)(r_{AU} + r_{UR}) + p_{AU} + p_{UR}^i]\} \delta_{AU}^i(t),$$

$$P_{UR}^i(t+1) = 2[f_R^i(t)r_{UR} + p_{UR}^i]\delta_{UU}^i(t) + [f_R^i(t)r_{AU} + p_{AU}] \delta_{AR}^i(t) + \{1 - [f_A^i(t)(r_{RU} + r_{UA}) + p_{RU} + p_{UA}^i]\} \delta_{UR}^i(t),$$

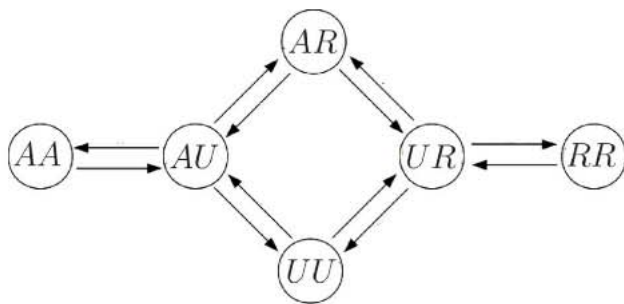


**Figure 2. Transitions for the 6-state model.** Transitions among the 6 distinct states in the 6-state model are indicated by arrows. The time step is supposed to be chosen small enough that only one site of the four nucleosome modification sites shown in Fig. 1 may change on each time step.

doi:10.1371/journal.pone.0077944.g002

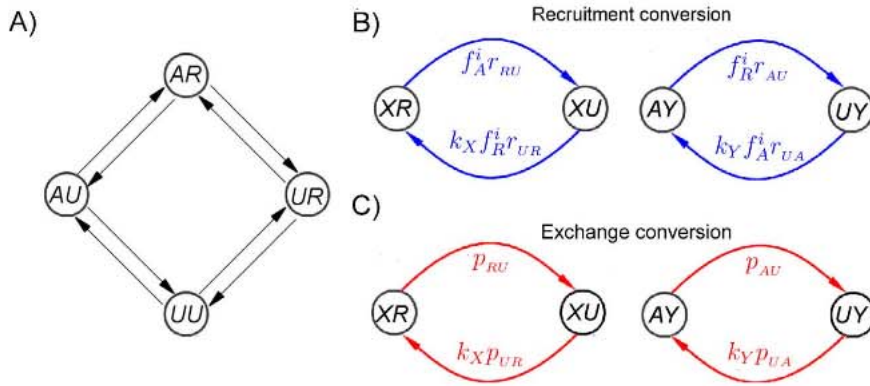


**Figure 3. Transitions for the reduced 4-state model.** (A) Transitions among the 4 distinct nucleosome states (i.e., AR, UR, AU, and UU) in the 4-state model. The time step is small enough that at most only one modification site of a nucleosome may change on each time step. (B) Transition probabilities between nucleosome states via recruitment conversions, where X can either be A or U while Y can either be R or U.  $k_X$  ( $k_Y$ ) = 2 if X (Y) is U, otherwise  $k_X$  ( $k_Y$ ) = 1. Thus, as an example, the transition probability from the AR state to the AU state is the same as that from the UR state to the UU state. (C) Transition probabilities between nucleosome states via exchange conversions, where X can either be A or U while Y can either be R or U.

doi:10.1371/journal.pone.0077944.g003

$$P_{AR}^i(t+1) = [f_R^i(t)r_{UR} + p_{UR}^i] \delta_{AU}^i(t) + [f_A^i(t)r_{UA} + p_{UA}^i] \delta_{UR}^i(t) + \{1 - [f_A^i(t)r_{RU} + f_R^i(t)r_{AU} + p_{RU} + p_{AU}]\} \delta_{AR}^i(t),$$

$$P_{UU}^i(t+1) = 1 - \{P_{AU}^i(t+1) + P_{UR}^i(t+1) + P_{AR}^i(t+1)\}.$$

Consistent with our assumption that at most one site on a nucleosome can change state in one time step, our choice of parameters satisfies  $r_{XY} p_{XY} \approx 1$ . Note that  $f_A^i(t)$  and  $f_R^i(t)$  depend on the lattice state in a neighborhood of site  $i$  within the range of recruitment specified in the first bullet above.

In section 4.3, where we treat localization of AR states, we allow the exchange transitions probabilities  $p_{XY}^i$  to vary from site to site, but everywhere else we consider  $p_{XY}^i$  to be the same at each site,  $p_{XY}^i = p_{XY}$ .

### Simulation Parameters

To assign roughly reasonable values to the parameters  $r_{XY}$  and  $p_{XY}$ , we first consider that our model time step,  $t \rightarrow t+1$ , corresponds to a real time step  $\Delta t = 2$  min. We have numerically verified that our simulation results are independent of our choice of  $\Delta t$  so long as  $\Delta t$  is sufficiently small. To estimate a rough range for the parameters  $r_{XY}$  and  $p_{XY}$ , we set  $p_{XY} r_{XY} \approx (\Delta t/T)$ , where  $T$  is the characteristic time scale of the relevant process (see Table 1), and, as required, the  $\Delta t$  that we have chosen is such that  $\Delta t/T$  is small compared to one for all such processes. We fix as many parameters (Table 1) as possible using experimental information (see Table 2). Because the authors are not aware of any experimental measurements of the characteristic time for recruitment demethylation and methylation via exchange, we will consider these probabilities as free parameters in our numerical simulations below. Previous work [32] suggests that the loss of active marks is faster than the loss of repressive marks. In particular, it has been shown that nucleosome turnover is faster in regions bound by trithorax-group proteins. Therefore, we selected the model parameters so that all rates associated with active mark are faster than those associated with the repressive mark.

Specifically, we assume that  $r_{UR}/r_{UA} = p_{UR}/p_{UA} = r_{RU}/r_{AU} = p_{RU}/p_{AU} = 0.5$  in the simulation (when nonzero). Regarding the cell cycle, for embryonic stem cells the cell cycle length is about 12 hours, which, with our  $\Delta t = 2$  min, corresponds to 360 time steps of our discrete time model per cell cycle. Finally, motivated by Ref. [31], we take  $l = 2$ , corresponding to a fairly short range of recruitment.

### Results

We now illustrate the utility of our model by employing it to investigate dynamic changes of histone modification patterns. As described in the Introduction, both nucleation sites and recruitment of methylation may be involved in the establishment of bivalent domains. As noted above, we suggest that certain nucleosomes act as nucleation sites during the early stages of development. These nucleation sites may be instrumental in the formation of bivalent domains. We incorporate nucleation sites into our model by assigning them a higher value of  $p_{UA}$  and  $p_{UR}$  than other sites, and we model the absence of nucleation sites by lowering its value of  $p_{UA}$  and  $p_{UR}$ .

In Sections 4.1 and 4.2, we discuss the formation and decay of AR states with different initial conditions in the absence of nucleation sites. In Section 4.3, we study the effect of nucleation sites on dynamics of the formation of AR states. Finally, in Section 4.4, we consider how varying the cell-cycle length affects AR states. Taken together, these analyses demonstrate the utility of our model for systematic investigation of the dynamic properties of bivalent domains.

#### 4.1 Formation of AR States

The formation of bivalent domains has been experimentally observed in studies of the early stages of embryogenesis [33] and in studies of cell reprogramming [34]. In particular, studies of cell reprogramming observe this formation process to be gradual [35].

In this section we use our model to simulate the formation of regions that are dense with AR states, and we identify such regions with bivalent domains. In the simulations, we take  $p_{UA} = p_{UR} = 0$  for all nucleosomes and fix  $r_{UA} = 0.046$  (corresponding to an H3K4me3 methylation timescale of 30 mins) and  $p_{AU} = 0.005$ . Also,  $r_{AU}$  and  $r_{RU}$  are considered to be very small (for simplicity, we set  $r_{AU} = r_{RU} = 0$ ), so that the AR states can be established and

**Table 1.** Summary of parameters.

Parameters	Physical description	Biological process simulated
$r_{UR}^i, r_{UA}^i$	Coefficient determining the probability of <i>U</i> converting to <i>R/A</i> via recruitment by the surrounding <i>R/A</i> marks	<b>Histone methylation spreading:</b> existing H3K27me3/H3K4me3 recruits methylase to methylate nearby nucleosomes.
$r_{RU}^i, r_{AU}^i$	Coefficient determining the probability of <i>R/A</i> converting to <i>U</i> via recruitment by the surrounding <i>R/A</i> marks	<b>Crosstalk between <i>A</i> and <i>R</i>:</b> existing H3K27me3/H3K4me3 recruits demethylase to demethylate nearby H3K4me3/H3K27me3.
$p_{UR}^i, p_{UA}^i$	Probability of <i>U</i> converting to <i>R/A</i> independent of the states of other nearby nucleosomes	<b>Nucleation:</b> continuous random histone marks placements at nucleosome site <i>i</i>
$p_{RU}^i, p_{AU}^i$	Probability of <i>R/A</i> converting to <i>U</i> independent of the states of other nearby nucleosomes	<b>Histone turnover rate:</b> histone marks can also be lost by random demethylation.
$f_{R>A}^i, f_{A>R}^i$	Fraction of <i>R/A</i> marks in nucleosomes within the recruitment range <i>l</i> of site <i>i</i>	We assume that the probability of recruitment (involved in the methylation spreading and crosstalk processes above) is proportional to the local density of the recruiting mark.
$\tau$	The cell-cycle DNA replication period	<b>Cell cycle</b>
<i>l</i>	The nucleosome interaction distance	<b>Recruitment Range</b>

doi:10.1371/journal.pone.0077944.t001

persist for a long time. For the initial state of the lattice in the simulations, we consider a situation where there are a relatively small number of nucleosomes in *AR* states, with all other nucleosomes initially in the *UU* state. In particular, we choose the initial number of *AR* nucleosomes to be five (out of the 80 nucleosomes on the lattice), and we study how *AR* states spread to other nucleosomes on the lattice. To investigate the effect of the initial spatial distribution of *AR* nucleosomes, we consider two extreme cases: *the localized case* in which all five initial *AR* state nucleosomes are located at five consecutive nucleosome sites in the center of the lattice, and *the delocalized case* in which the five initial *AR* state nucleosomes are located at equally spaced sites spanning the entire lattice (at sites 1, 20, 40, 60, 80).

Fig. 4 shows results for the space-time evolution of the distribution of nucleosomes for both *localized* (left column of figure panels) and *delocalized* (right column of figure panels) initial states. Fig. 4C shows space-time plots for the four types of nucleosomes in a typical single run, while Figs. 4A–B show average space-time plots of the level of *AU* and *AR* nucleosomes, that is, the fraction of runs for which the nucleosome is in the indicated state. The average level of *UR* nucleosomes (not plotted) is low everywhere all the time (dark blue, in terms of the color scale of Figs. 4A and B). Note that, in Figs. 4A–B, the regular drops of the levels of the indicated nucleosomes every 360 time steps (corresponding to the start of a new cell cycle) are due to the inserted of *UU* nucleosomes in the DNA replication process. In Fig. 4A, for the localized case (corresponding to the left panel figure), the *AR* nucleosomes spread over the lattice via a propagating front [27] manifested by the approximately straight lines of the color transition boundaries emanating from the space-time point at the center of the lattice at time  $t = 0$ . For the delocalized case (right panel of Fig. 4A), *AR* nucleosomes spread over the lattice via individual propagating fronts emanating from the five initial *AR* sites. These fronts merge near the end of the first cell-cycle (time  $\approx 300$ ), but the system takes longer time (time  $\approx 1250$ ) to reach a final equilibrium distribution. The model results show that, while the space time evolution of the distribution of *AR* nucleosomes is dependent upon the initial condition, the time it takes to establish a final equilibrium distribution is comparable and relatively long for both the localized and delocalized cases. This may have

relevance to the experimental observation of Ref. [35] that the establishment of bivalent domains is gradual.

For the localized case, there appears to be two fronts, a fast  $UU \rightarrow AU$  front (corresponding to the blue to yellow transition in the left panel of Fig. 4C), followed by a  $AU \rightarrow AR$  front (yellow to red transition in the left panel of Fig. 4C) that propagates at a slower speed than the  $UU \rightarrow AU$  front. The slow  $AU \rightarrow AR$  front is clearly seen in the left panels of Figs. 4A and B, while the  $UU \rightarrow AU$  front is evident in the left panel of Fig. 4B. These two fronts propagate symmetrically in space in the average space-time plots (Fig. 4A and 4B) but, due to fluctuations, more asymmetrically in space in the single run plot (see left panel of Fig. 4C). Examining a range of parameters, we find that the fastest front corresponds to either a  $UU \rightarrow AU$  transition (as in Fig. 4B) or a  $UU \rightarrow RU$  transition (not shown). For the delocalized case, we also observe that the spreading of the active marks is faster than that of the repressive marks. This can be easily seen from the typical single run plot in the right panel of Fig. 4C.

Finally, we also studied the effects of varying the number of *AR* nucleosomes in the initial condition on the above simulations. Using the same parameters values as above, we plot (Fig. 5) the final average fraction of *AR* nucleosome at the end of the final simulated cell cycle (10 cell cycles) as function of the initial number *m* of *AR* nucleosomes which are taken to occupy the *m* nucleosome sites in the center of the lattice. As shown in Fig. 5, the average fraction of final *AR* nucleosomes initially increases with increasing *m*. We observe that past  $m \approx 4$  (i.e.,  $m/80 \approx 0.05$ ) the value is essentially constant up to  $m = 80$  with *AR* nucleosomes spanning the whole lattice. For a given *m*, each simulation can be categorized into two groups, (1) the final spatial average level of *AR* nucleosomes is approximately equal to the corresponding large *m* limiting value, or (2) all *AR* nucleosomes vanish. Thus at low *m*, the value plotted on the vertical axis of Fig. 5 can be thought of as the limiting larger-*m* value (basically the value at  $m = 4$ ) multiplied by the fraction of runs in category (1). In the early stage of a simulation, the spreading of histone marks compete with the loss of histone marks via histone turnover. If either type of mark is lost totally, it cannot recover (i.e., the run is in category 2). On the other hand, we find that histone marks do not die out if there are enough of them on the lattice (the run is then in category 1). As a result, the average fraction of *AR* nucleosomes is larger

**Table 2.** Model parameters.

Dynamical processes	Parameters	Characteristic time	References
Adding H3K4me3 marks via recruitment	$r_{UA}$	0.5–6 hours	[38,39]
Adding H3K27me3 marks via recruitment	$r_{UR}$	0.5–6 hours	[38,39]
Removing both H3K4me3 and H3K27me3 marks via exchange	$p_{AU}$ and $p_{RU}$	1–24 hours	[38,39]
Adding both H3K4me3 and H3K27me3 marks via exchange	$p_{UA}$ and $p_{UR}$	not known	-----
Removing both H3K4me3 and H3K27me3 marks via Recruitment	$r_{AU}$ and $r_{RU}$	not known	-----
Cell cycle length in human embryonic stem cells	$\tau$	12 hours	[40]
Cell cycle length in human adult cells	$\tau$	24 hours	[40]

doi:10.1371/journal.pone.0077944.t002

with larger  $m$ , and with smaller  $p_{AU}$  and  $p_{RU}$  (compare the red and blue plots in Fig. 5). The above simulations suggest that in order for  $AR$  states to form when  $p_{UA}$  and  $p_{UR}$  are small, a sufficient number of initial  $AR$  nucleosomes is required. Taken together, these results have shown that the formation of bivalent domains undergoes two distinct phases: expansion and stabilization. In the expansion phase, the border of bivalent domains expands to neighboring nucleosomes. The expansion process is relatively fast (w 10 nucleosomes per cell-cycle in our simulation) but quite noisy. As a result, only a sparse subset of nucleosomes are marked with the  $AR$  state. During the stabilization phase, the nucleosome state configuration is further refined and eventually reaches an equilibrium. Even then, the state of individual nucleosomes is still highly dynamic and equilibrium is only reached in the statistical sense.

#### 4.2 Decay of AR States

In this section we use our model to simulate the decay of  $AR$  states. All parameters are the same as in section 4.1 except that  $r_{AU}$  and  $r_{RU}$  are taken to be non-zero. This is motivated by experimental findings that recruitment of demethylases is important for the decay of bivalent domains [22,23], and occurs during cell differentiation. Also, we consider an initial condition in which all nucleosomes are in  $AR$  states. Results are shown in Figs. 6, 7, and 8 for different values of  $r_{AU}$  and  $r_{RU}$  keeping their ratio fixed at  $r_{AU}/r_{RU} = 2$ .

Fig. 6 shows results for the space-time evolution of the distribution of all four nucleosome states  $AR$ ,  $UR$ ,  $AU$ , and  $UU$  for three values of  $r_{AU} : 2r_{RU}$ . In Fig. 6A, for the case  $r_{AU} = 0.004$ , the initial level of  $AR$  nucleosomes rapidly (in about one cell-cycle) drops to a lower level of  $AR$  nucleosomes, but there still remains a substantial presence of  $AR$  nucleosomes which persists to the end of the run. In contrast, for both  $r_{AU} = 0.016$  and  $r_{AU} = 0.034$ , where there is again similar very rapid decreases of the level of  $AR$  nucleosomes, now the final level is essentially zero. In addition, it is seen that the level of  $AR$  nucleosomes takes longer to fully decay for  $r_{AU} = 0.016$  than for  $r_{AU} = 0.034$ . The latter case is consistent with the experimental observations [10,35] that an essentially complete loss of bivalent domain can occur very rapidly. To further explore how the decay of  $AR$  states depends on the recruitment demethylation rates, we plot the fraction of simulation runs that have at least one  $AR$  nucleosome on the lattice as a function of time in Fig. 7, and the final average fraction of  $AR$  nucleosomes (averaged over 1000 runs) as a function of  $r_{AU}$  in Fig. 8. Comparing Fig. 6A to Fig. 7, we observe that the fraction of runs with at least one  $AR$  nucleosome plotted in Fig. 7 shows a slower decay compared to the decay of  $AR$  levels in Fig. 6A. This suggests that lineage-control genes in bivalent domains may

become active without the full destruction of repressive marks. In Fig. 8, as might be anticipated, we observe that, in general, smaller histone turnover ( $p_{AU}$ ) and smaller recruitment demethylation rate give a higher final average fraction of  $AR$  nucleosomes. Also, the value of  $r_{AU}$  at which the average fraction of  $AR$  nucleosomes drops to zero is lower for larger  $p_{AU}$ . Our results suggest that a large recruitment demethylation rate in a cell is important for cell differentiation. This is consistent with experimental findings [22,23].

In a real situation, a change from low to high values of the recruitment demethylation rates during cell differentiation will take place by processes not included in our model, and these processes may take some time. Thus our simulation use of constant non-zero initial  $r_{AU}$  and  $r_{RU}$  results in a determination of the characteristic decay time associated only with processes that are included in our model, and the true decay rate of  $AR$  state nucleosomes may be longer than this time due to the finite time for  $r_{AU}$  and  $r_{RU}$  to change. Overall, we observe that the decay determined from our model of  $AR$  state nucleosomes in response to high initial value of recruitment demethylation rate is relatively fast, as compared to the time that it takes to establish  $AR$  states spanning the lattice in Section 4.1. We conclude from this that processes included in our model do not prevent rapid decay of  $AR$  state nucleosomes, and that rapid decay, as seen in experiments [10], can occur in response to rapid increase of  $r_{AU}$  and  $r_{RU}$ .

In addition, it is interesting to emphasize the probabilistic nature of these results. For example, Fig. 6D shows results of typical single realizations. This figure also shows that the final state for  $r_{AU} = 0.016$  is different from that for  $r_{AU} = 0.034$ . For the case  $r_{AU} = 0.016$ , we observe that  $AU$  nucleosomes are dominant in the lattice at the end of the simulation (see also the second panels of Figs. 6B and 6C). However, for the case of  $r_{AU} = 0.034$  at long time, green regions of  $UR$  nucleosomes form at the upper edge (see third panel of Fig. 6D), while the  $AU$  nucleosomes are at the lower edges. This is because the  $AU$  and  $UR$  states can both be stable for this combination of parameters (see third panels of Figs. 6B and 6C). Our results suggest that the strength of the recruitment demethylation (i.e., the values of  $r_{AU}$  and  $r_{RU}$ ) is not only important for the decay of bivalent domains, but also strongly influences the possible final state following decay.

#### 4.3 The localization of AR States

The next issue that we discuss is the effect of nucleation sites (i.e., in our model,  $p_{UA} = p_{UR} = 0$  at these sites). The existence of such sites is suggested by the finding [4,25] that DNA specific sequences can recruit protein binding factors like transcription factor which in turn recruit histone marks to the DNA. In section 4.1, we took  $p_{UA} = p_{UR} = 0$ , and we found that  $AR$  nucleosomes

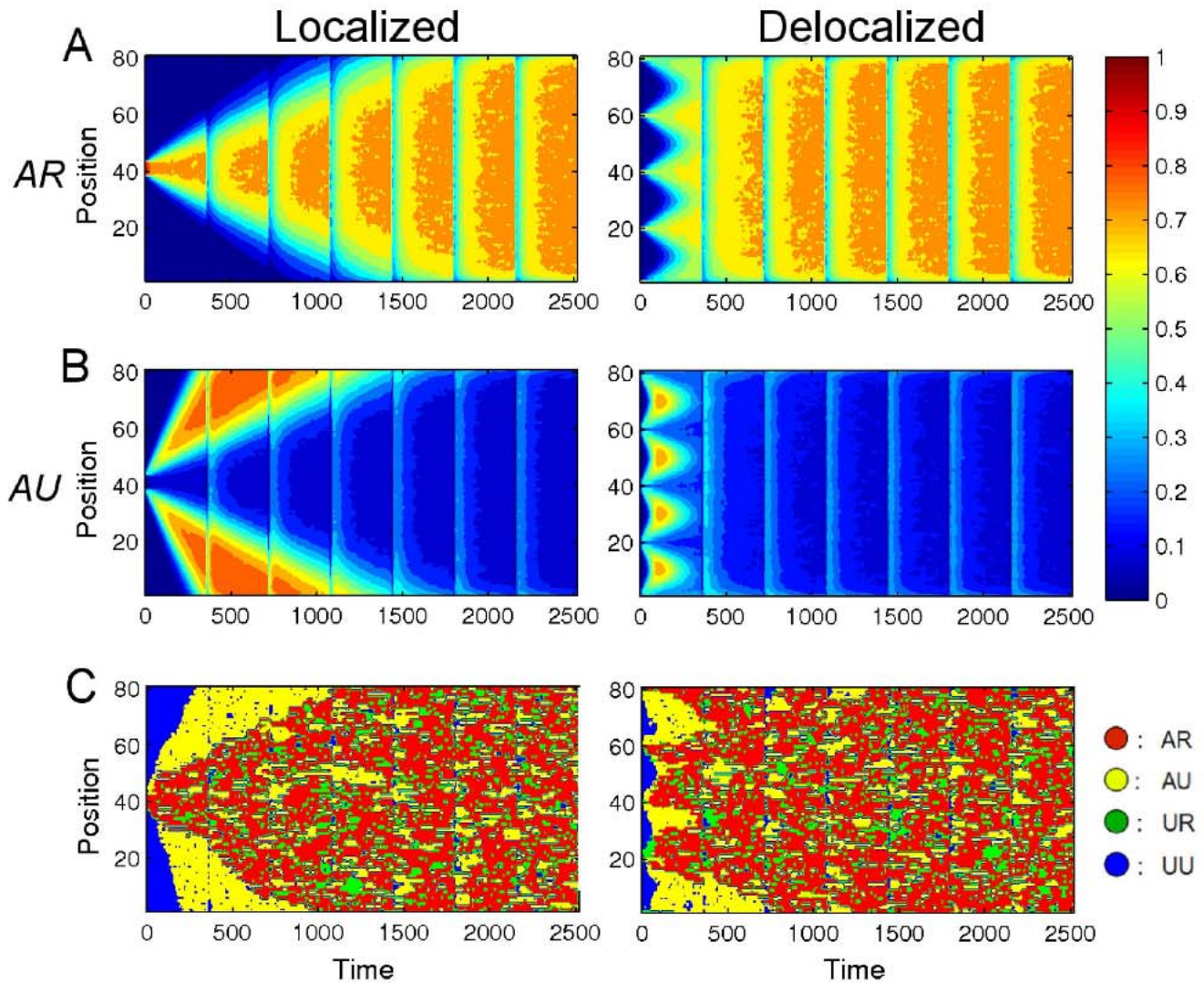


**Figure 4. Space-time plots for the formation of *AR* states.** Space-time plots of the average level of *AR* and *AU* nucleosomes for the localized and delocalized initial conditions are shown in (A) and (B). Here by 'level' we mean the fraction of runs for which the nucleosome is in the indicated state. These levels are computed by counting the indicated type of nucleosome in all runs at each position and time, and averaging over 2000 runs. The red color indicates a higher level of the indicated type of nucleosome while the blue color indicates a lower level of that type of nucleosome. (C) Space-time plots for a single run for the localized and delocalized initial conditions. *AR*, *AU*, *UR*, and *UU* nucleosomes are plotted in red, yellow, green, and blue, respectively.  
doi:10.1371/journal.pone.0077944.g004

either span the whole lattice or disappear. Although similar broad bivalent domains are observed, narrow bivalent domains are also detected in some experiments [3,24]. A recent model [11] has previously been used to simulate the dynamics of localized histone modification domains, but that model allowed only a single type of histone modification, and therefore it cannot address the dynamics of bivalent domains. Using our model, we will be able to analyze interactions among the placements of active and repressive histone marks, histone turnover rate, and crosstalk between active and repressive histone marks. We consider  $p_{UA}$  and  $p_{UR} \ll 0$  for the central nucleosome (corresponding to the case that the central nucleosome is a nucleation site). For the initial condition, we consider that there are five *AR* nucleosomes located at the five consecutive nucleosome sites in the center of the lattice, with all other nucleosomes initially in *UU* state. Using our previous parameter ratios (i.e.,  $r_{UR}/r_{UA} = p_{UR}/p_{UA} = r_{RU}/r_{AU} = p_{RU}/p_{AU} =$

0.5), we explore the parameter space regions for which our model reproduces narrow and broad distributions of *AR* nucleosomes.

We consider cases of both relatively small and relatively large recruitment demethylation rates ( $r_{AU}$  and  $r_{RU}$ ). The former and latter choices are meant to simulate cell environments far before, and during, cell differentiation, respectively. We run the simulations for four cell-cycles such that the averaged nucleosome state configuration reaches an equilibrium. In particular, a steady spatial distribution of *AR* nucleosomes seems to be reached within the first cell-cycle, and change very little thereafter. Therefore, the time for establishment of a highly localized *AR* distribution ( $\approx 1$  cell-cycle) is much shorter compared to that of establishing a very broad and uniform *AR* distribution (about 5 cell-cycles and see Figure 4A). For the case of small recruitment demethylation rate, Figs. 9A–B show plots of the fraction of *AR* nucleosomes averaged over 2000 simulations. Figs. 9A–B demonstrate narrow (left panels of Figs. 9A and 9B) and broad (right panels of Figs. 9A and 9B)

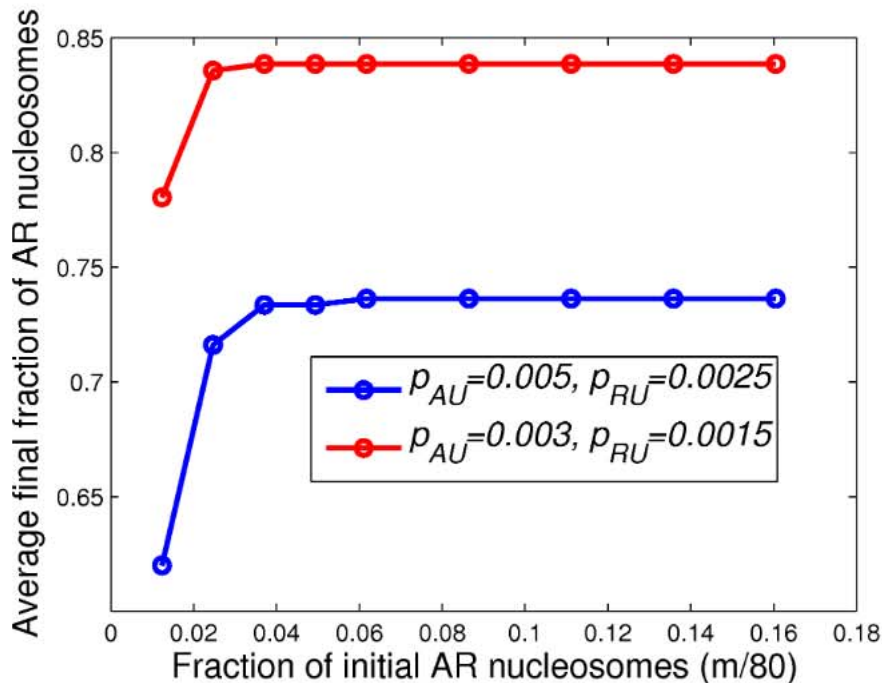


**Figure 5. Average final fraction of *AR* nucleosomes vs. the number of initial *AR* nucleosomes.** The average final fraction of *AR* nucleosomes is plotted as a function of  $m$  (the number of initial *AR* nucleosomes) for  $(p_{AU}, p_{RU})$  being (0.003, 0.0015)(red) and (0.005, 0.0025)(blue). These levels of *AR* nucleosomes are computed by averaging the final number of *AR* nucleosomes in the simulations over 2000 runs. doi:10.1371/journal.pone.0077944.g005

distributions of *AR* nucleosomes. The widths of these bounded distributions reflect the balance between the continuous placement of histone marks on the nucleation site, the spreading of histone marks by the recruitment process, and the destruction of histone marks via exchange [11]. From the simulations, we find that the width of the distributions of *AR* nucleosomes depends more on  $p_{AU}$  and  $p_{RU}$ , which they are inversely related to the width of the *AR* distribution. On the other hand, the amplitude of the distributions depends more on  $p_{UA}$  and  $p_{UR}$  (i.e., the continuous placements of histone marks on the center nucleosome) (Figs. 9A–B).

Next, we did simulations using the same parameters as in Fig. 9A but with larger recruitment demethylation rates ( $r_{AU}$  and  $r_{RU}$ ). The results are shown in Fig. 9C. Both of the corresponding distributions in Fig. 9A become narrower in Fig. 9C. In particular, the changes in the broad distribution (right panel) is particularly dramatic. This suggests that it may be easier to see changes in the broad bivalent domain than the narrow one during cell differentiation in experiments. Overall, our results demonstrate that nucleation sites can be responsible for the onset of bounded domains of *AR* nucleosomes. Also, narrow distributions can be obtained via either enhanced histone demethylation via exchange or via enhanced recruitment. We have also studied the distributions of *AR* nucleosomes, active marks, and repressive marks, using other reasonable parameter choices (see Figure S2 and the corresponding texts in Text S1). Taken together, these results suggest that highly localized bivalent domain patterns can be established surrounding nucleation sites, similar to the one-mark scenario described in previous study [11]. However, the local dynamics is more complex because multiple states are involved in the competition. The end configuration is an equilibrium resulting from the balance of multiple molecular forces.

#### 4.4 The Effects of Cell-cycle Length on the Stability of *AR* States

During DNA replication, the nucleosomes, along with their associated histone marks, must be dissociated from the mother strand. How these marks are reassembled to the newly synthesized strands remains poorly understood. Recent studies suggest that the nucleosome, along with their associated marks, are randomly distributed to daughter strands [31]. In this section, we use our model to study the impact of DNA replication on the level of *AR* nucleosomes.

We choose parameters which correspond to cell environments during the formation of bivalent domains (see Fig. 10). Also, we assume that nucleation sites lose their properties at the very beginning of the simulations, so that there are no nucleation sites. We then vary the cell cycle lengths from 6 hours to 24 hours, which corresponds to varying the cell cycle length from that in stem cell to that in differentiated cells. We run the simulations for 10 cell cycles such that the average level of *AR* nucleosomes over a cell cycle reaches a stable value. Fig. 10 shows the average level of *AR* nucleosomes as a function of cell cycle length, where these levels are computed by averaging the number of *AR* nucleosomes at the end of the simulations over the lattice and over all simulation runs. Fig. 10 shows that the average level of *AR* nucleosomes is, in general, larger for longer cell-cycle. This result is expected, since there is more time for the lattice to recover from the loss of *AR* nucleosomes, caused by DNA replication, when the cell-cycle is longer. But the significance of cell-cycle length seems to be weaker for strong bivalent domains (blue curve in Fig. 10). This result is consistent with the experimental finding that higher levels of histone marking are observed when the length of the cell cycle increases [36].



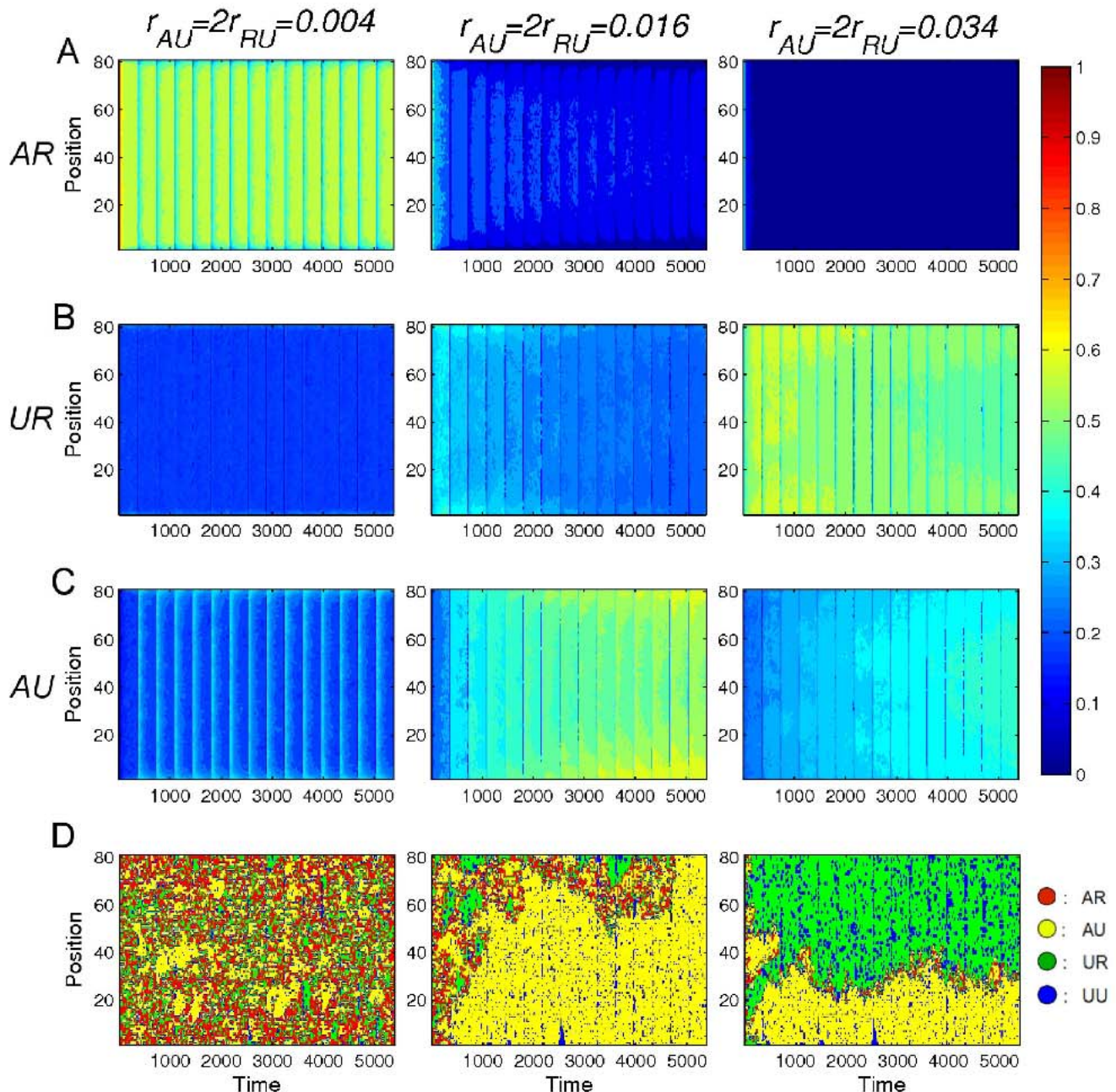


**Figure 6. Space-time plots for the decay of *AR* states.** In these plots, all nucleosomes are initially ( $t=0$ ) in the *AR* state. Space-time plots of the average level of *AR*, *UR*, and *AU* nucleosomes for  $r_{AU}=0.004, 0.016$ , and  $0.034$  are shown in (A), (B), and (C), respectively. These plots are similar to Figure 4A and B. Here by level we mean the fraction of runs for which the nucleosomes is the indicated state. (D) Space-time plots for a single run with  $r_{AU}=0.004, 0.016, 0.034$ . *AR*, *AU*, *UR*, and *UU* nucleosomes are plotted in red, yellow, green, and blue, respectively.  
doi:10.1371/journal.pone.0077944.g006

## Discussion

Development of computational models of bivalent domain dynamics can help to elucidate the mechanism of chromatin domain formation, and give insight for formulating and analyzing experimental studies. In this paper we introduce a model that incorporates multiple histone marks on a nucleosome and the interactions among these marks. We have illustrated the potential use of our model by employing it to investigate the dynamics of bivalent domains, with the following results.

Our main conclusion is that the formation of bivalent domains are highly stochastic at individual nucleosomes, but reproducible patterns can be obtained by averaging a large number of simulations. Dynamic changes of these patterns are maintained by the subtle balance of the multiple factors including the exchange rate, recruitment, distribution of nucleation sites, and cell-cycle length, resulting high degree of plasticity which might be advantageous for facilitating smooth transitions between cell-states during development.

Our analysis suggests that the formation of bivalent domains is in general a slow, two-step process, which can be divided into an

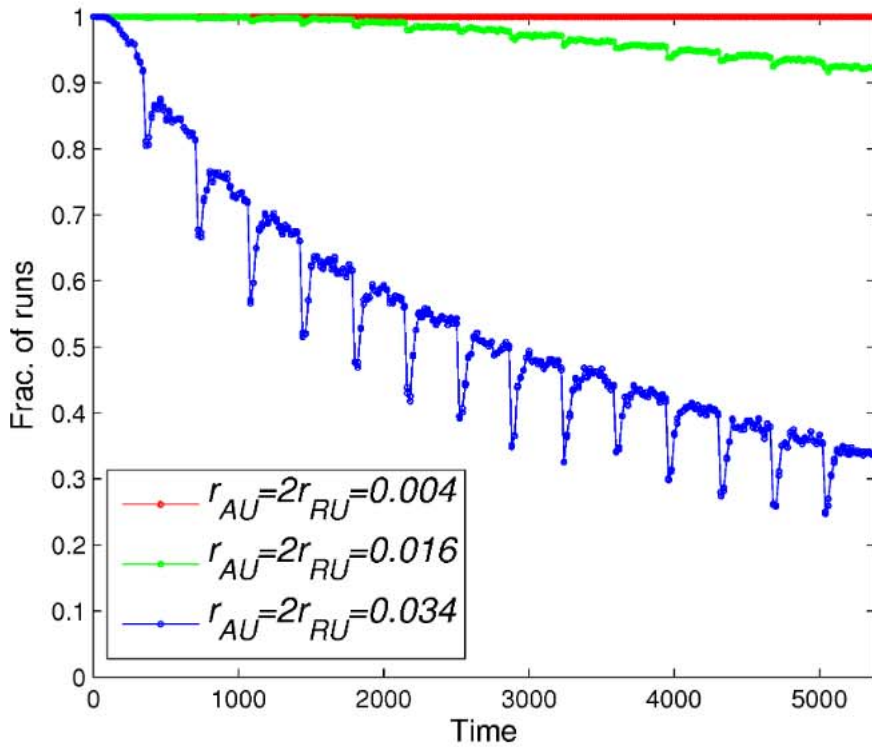


**Figure 7. Fraction of runs that have at least one AR nucleosome vs. time.** The fraction of runs that have at least one AR nucleosome on the lattice is plotted as a function of time for  $r_{AU} = 0.004, 0.016,$  and  $0.034$ .  
doi:10.1371/journal.pone.0077944.g007

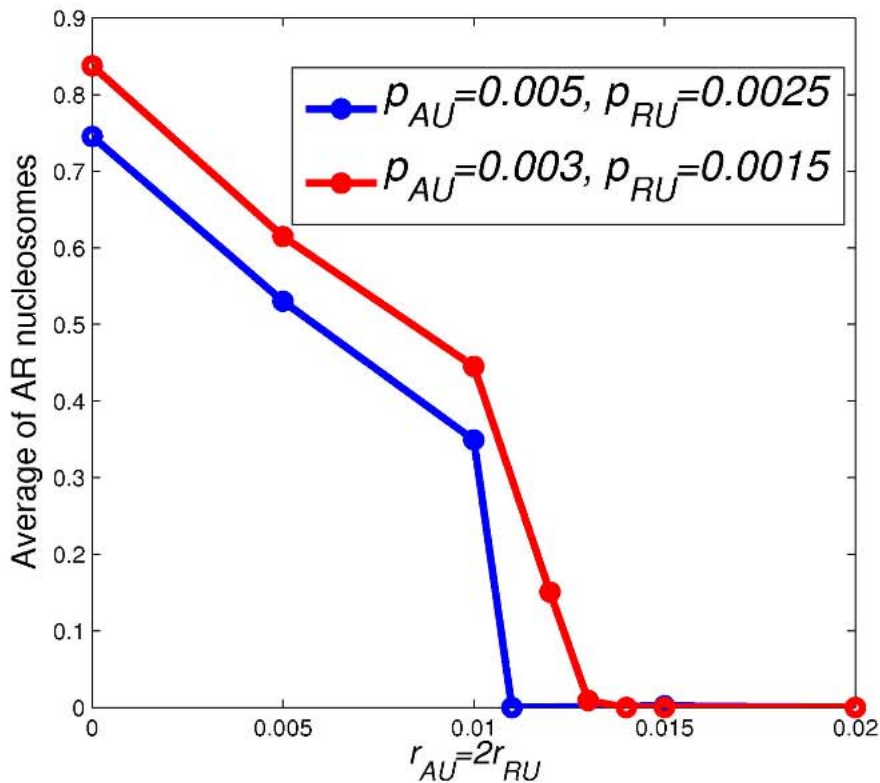


**Figure 8. Average level of AR nucleosomes vs.  $r_{AU}$ .** The average level of AR nucleosomes is plotted as a function of  $r_{AU}$  for both  $p_{AU} = 0.003$  and  $0.005$ . These levels of AR nucleosomes are computed by averaging the final number of AR nucleosomes in the simulations over all the runs and the whole lattice.  
doi:10.1371/journal.pone.0077944.g008

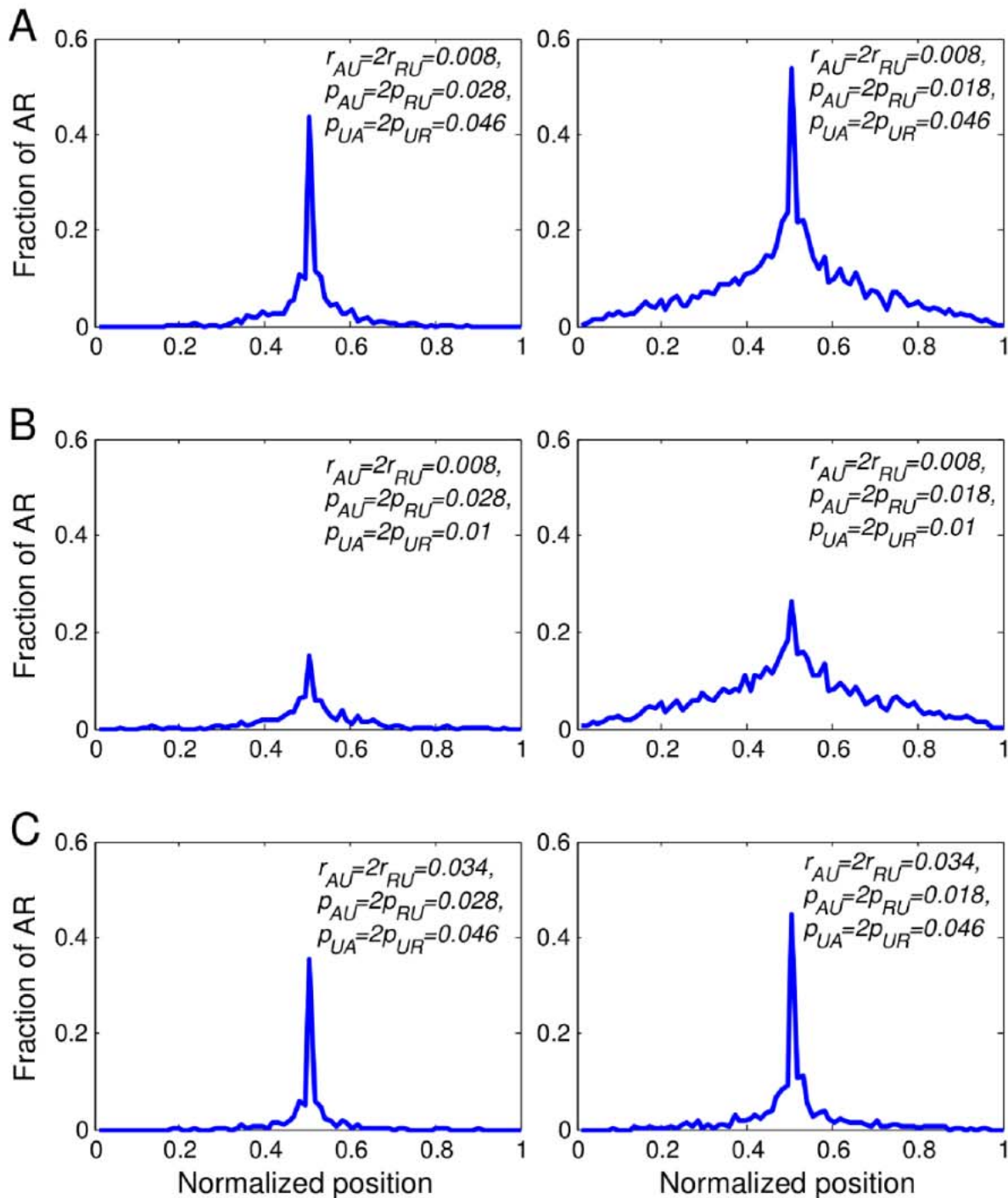


**Figure 9. Distributions of AR nucleosomes.** Distributions of AR nucleosomes are plotted at the final time of the simulations (time = 1800). doi:10.1371/journal.pone.0077944.g009

expansion and a stabilization phase. In contrast, the decay of bivalent domains, induced by demethylase activities, is much faster. This asymmetry between formation and decay dynamics may be an important feature for development control and perhaps needs to be taken into consideration into development epigenetic-based therapeutic approaches.

Specific epigenetic patterns can be established through targeted recruitment of chromatin regulators to specific genomic sequences. The effect of such nucleation sites on the establishment of highly

localized epigenetic patterns has been studied via computational models in a number of previous studies [11,37]. We have extended these investigations by considering multiple histone marks in our model. As expected, we found that the strength of a nucleation site plays an important role in maintenance of localized bivalent domains. In the absence of nucleation sites, the bivalent domains either expands to the whole nucleosome array or disappears entirely. Our analysis is consistent with numerous experiment

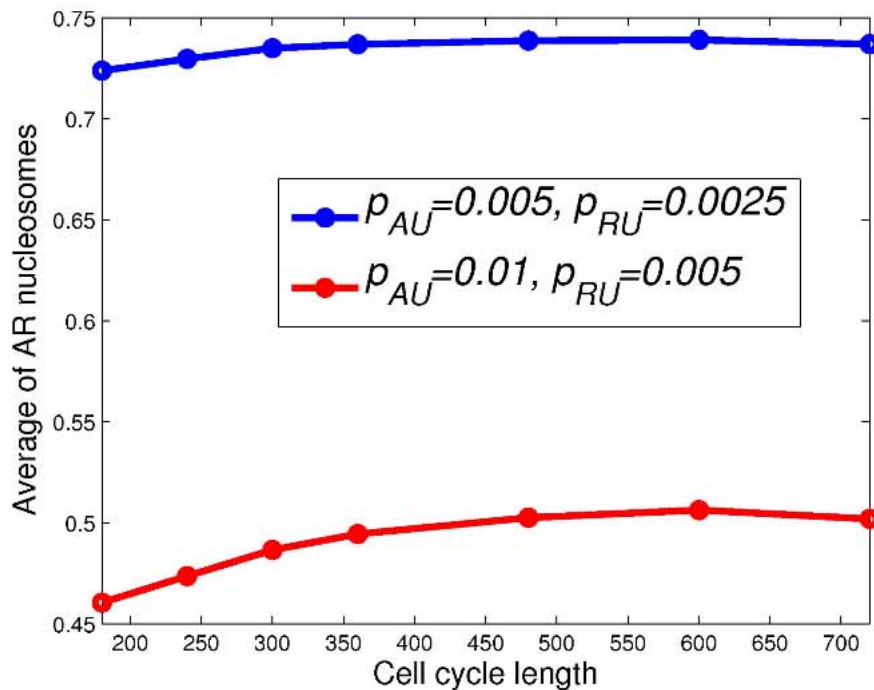


**Figure 10. Average AR nucleosome level vs. cell-cycle length.** The average AR nucleosome level is plotted as a function of cell-cycle length. These levels of AR nucleosomes are computed by averaging the final number of AR nucleosomes in the simulations over all the runs and the whole lattice.  $r_{UA} = 2r_{UR} = 0.046$ ,  $p_{UA} = p_{UR} = 0$ , and  $r_{AU} = r_{RU} = 0$ . doi:10.1371/journal.pone.0077944.g010

studies, which show that GC-rich DNA sequences are required for establishment of bivalent domains [26].

One limitation of our current model is that many kinetic parameters remain unknown, preventing us from making more quantitative predictions. Nevertheless, the major conclusions described above are robust with respect to parameter value changes therefore may reflect true biological principles. It will be interesting to test these principles by conducting quantitative experimental measurements.

## Supporting Information

Figure S1 Illustration for the explanation of the states of the 6-state model. (TIFF)

Figure S2 An example of the distribution of AR nucleosomes, active, and repressive marks. This plot illustrates that the 4-state model described in the main text can simulate bivalent domains (blue) in which the active mark (green) is less extensive than the repressive mark (red) (i.e., the bivalent domains (blue) are buried in the repressive domains (red)). The details of simulation can be referred to Section 4.3 in the main text. Here, distributions of AR nucleosomes (blue), AR+UR

nucleosomes (red), and AR+AU nucleosomes (green) are plotted at the end of the simulation runs (time = 1800). The average levels of nucleosomes are averaged over 1000 simulation runs. In the simulation,  $p_{UA}^{i=40} = 0.03$  and  $p_{UR}^{i=40} = 0.015$ . The other parameters are  $r_{UA} = 0.029$ ,  $r_{UR} = 0.021$ ,  $p_{AU} = 0.025$ ,  $p_{RU} = 0.015$ ,  $r_{AU} = 0.004$  and  $r_{RU} = 0.002$ .

(TIFF)

Text S1 The supplementary text provides details regarding the formulation of our model and another example of localization of AR states related to our results in Section 4.3.

(PDF)

## Acknowledgments

We thank Nicole Francis and Shane Squires for discussions.

## Author Contributions

Conceived and designed the experiments: WLK MG GCY FS EO. Performed the experiments: WLK. Analyzed the data: WLK MG GCY FS EO. Wrote the paper: WLK MG GCY FS EO.

## References

- Kouzarides T (2007) Chromatin modifications and their function. *Cell* 128: 693–705.
- Jenuwein T, Allis CD (2001) Translating the histone code. *Science* 293: 1074–1080.
- Mikkelsen TS, Ku M, Jaffe DB, Issac B, Lieberman E, et al. (2007) Genome-wide maps of chromatin state in pluripotent and lineage-committed cells. *Nature* 448: 553–560.
- Moazed D (2011) Mechanisms for the inheritance of chromatin states. *Cell Press* 146: 510–518.
- Kouzarides T (2007) Chromatin modifications and their function. *Cell* 128: 693–705.
- Bernstein BE, Mikkelsen TS, Xie X, Kamal M, Huebert DJ, et al. (2006) A Bivalent Chromatin Structure Marks Key Developmental Genes in Embryonic Stem Cells. *Cell* 125: 315.
- Zhao XD, Han X, Chew JL, Liu J, Chiu KP, et al. (2007) Whole-genome mapping of histone h3 lys4 and 27 trimethylations reveals distinct genomic compartments in human embryonic stem cells. *Cell Stem Cell* 1: 286–298.

8. Pan G, Tian S, Nie J, Yang C, Ruotti V, et al. (2007) Whole-genome analysis of histone h3 lysine 4 and lysine 27 methylation in human embryonic stem cells. *Cell Stem Cell* 1: 299–312.
9. Vastenhouw NL, Schier AF (2012) Bivalent histone modifications in early embryogenesis. *Current Opinion in Cell Biology* 24: 374–386.
10. Chakravarthy H, Ormsbee BD, Mallanna SK, Rizzino A (2011) Rapid activation of the bivalent gene *sox21* requires displacement of multiple layers of gene-silencing machinery. *The FASEB Journal* 25: 206–218.
11. Hodges C, Crabtree GR (2012) Dynamics of inherently bounded histone modification domains. *Proceedings of the National Academy of Sciences* 109: 13296–13301.
12. Dodd IB, Micheelsen MA, Sneppen K, Thon G (2007) Theoretical analysis of epigenetic cell memory by nucleosome modification. *Cell* 129: 813–822.
13. David-Rus D, Mukhopadhyay S, Lebowitz JL, Sengupta AM (2009) Inheritance of epigenetic chromatin silencing. *Journal of Theoretical Biology* 258: 112–120.
14. Sedighi M, Sengupta AM (2007) Epigenetic chromatin silencing: bistability and front propagation. *Physical Biology* 4: 246.
15. Ringrose L, Paro R (2007) Polycomb/trithorax response elements and epigenetic memory of cell identity. *Development* 134: 223–232.
16. Ku M, Koche RP, Rheinbay E, Mendenhall EM, Endoh M, et al. (2008) Genomewide analysis of *prc1* and *prc2* occupancy identifies two classes of bivalent domains. *PLoS Genet* 4: e1000242.
17. Margueron R, Justin N, Ohno K, Sharpe M, Son J, et al. (2009) Role of the polycomb protein *eed* in the propagation of repressive histone marks. *Nature* 461: 762–767.
18. Hansen K, Bracken A, Pasini D, Dietrich N, Gehani S, et al. (2008) A model for transmission of the h3k27me3 epigenetic mark. *Nature Cell Biology* 10: 1291–1300.
19. Orlando DA, Guenther MG, Frampton GM, Young RA (2012) CpG island structure and trithorax/polycomb chromatin domains in human cells. *Genomics* 100: 320–326.
20. Welstead GG, Creyghton MP, Bilodeau S, Cheng AW, Markoulaki S, et al. (2012) X-linked h3k27me3 demethylase *utx* is required for embryonic development in a sex-specific manner. *Proceedings of the National Academy of Sciences* 109: 13004–13009.
21. Kooistra S, Helin K (2012) Post-translational modifications: Molecular mechanisms and potential functions of histone demethylases. *Nature Reviews Molecular Cell Biology* 13: 297–311.
22. Pasini D, Hansen KH, Christensen J, Agger K, Cloos PA, et al. (2008) Coordinated regulation of transcriptional repression by the *rbp2* h3k4 demethylase and polycomb-repressive complex 2. *Genes Development* 22: 1345–1355.
23. Cloos PA, Christensen J, Agger K, Helin K (2008) Erasing the methyl mark: histone demethylases at the center of cellular differentiation and disease. *Genes Development* 22: 1115–1140.
24. Kim SW, Yoon SJ, Chuong E, Oyolu C, Wills AE, et al. (2011) Chromatin and transcriptional signatures for nodal signaling during endoderm formation in hescs. *Developmental Biology* 357: 492–504.
25. Yuan GC (2012) Linking genome to epigenome. *WIREs Syst Biol Med* 4: 297–309.
26. Mendenhall EM, Koche RP, Truong T, Zhou VW, Issac B, et al. (2010) Gc-rich sequence elements recruit *prc2* in mammalian es cells. *PLoS Genet* 6: e1001244.
27. Sedighi M, Sengupta AM (2007) Epigenetic chromatin silencing: bistability and front propagation. *Physical Biology* 4: 246.
28. Binder H, Steiner L, Przybilla J, Rohlf T, Prohaska S, et al. (2013) Transcriptional regulation by histone modifications: towards a theory of chromatin re-organization during stem cell differentiation. *Physical Biology* 10: 026006.
29. Sneppen K, Dodd IB (2012) A simple histone code opens many paths to epigenetics. *PLoS Comput Biol* 8: e1002643.
30. Voigt P, LeRoy G, Drury WJ III, Zee B, Son J, et al. (2012) Asymmetrically modified nucleosomes. *Cell* 151: 181–193.
31. Radman-Livaja M, Verzijlbergen KF, Weiner A, van Welsom T, Friedman N, et al. (2011) Patterns and mechanisms of ancestral histone protein inheritance in budding yeast. *PLoS Biol* 9: e1001075.
32. Deal RB, Henikoff JG, Henikoff S (2010) Genome-wide kinetics of nucleosome turnover determined by metabolic labeling of histones. *Science* 328: 1161–1164.
33. Vastenhouw N, Zhang Y, Woods I, Imam F, Regev A, et al. (2010) Chromatin signature of embryonic pluripotency is established during genome activation. *Nature* 464: 922–926.
34. Wernig M, Meissner A, Foreman R, Brambrink T, Ku M, et al. (2007) In vitro reprogramming of fibroblasts into a pluripotent es-cell-like state. *Nature* 448: 318–324.
35. Polo JM, Anderssen E, Walsh RM, Schwarz BA, Nefzger CM, et al. (2012) A molecular roadmap of reprogramming somatic cells into ips cells. *Cell* 151: 1617–1632.
36. Calder A, Roth-Albin I, Bhatia S, Pilquil C, Lee JH, et al. (2013) Lengthened g1 phase indicates differentiation status in human embryonic stem cells. *Stem Cells and Development* 22: 279–295.
37. Hathaway NA, Bell O, Hodges C, Miller EL, Neel DS, et al. (2012) Dynamics and memory of heterochromatin in living cells. *Cell* 149: 1447–1460.
38. Zee B, Levin R, DiMaggio P, Garcia B (2010) Global turnover of histone post-translational modifications and variants in human cells. *Epigenetics and Chromatin* 3: 22.
39. Zee BM, Levin RS, Xu B, LeRoy G, Wingreen NS, et al. (2010) In vivo residue-specific histone methylation dynamics. *Journal of Biological Chemistry* 285: 3341–3350.
40. Orford K, Scadden D (2008) Deconstructing stem cell self-renewal: Genetic insights into cell-cycle regulation. *Nature Reviews Genetics* 9: 115–128.

